Effect of tip gap size on the performance of an axial compressor stage with and without active flow control

Clémence Rannou, Julien Marty, Geoffrey Tanguy, Antoine Dazin

EFFECT OF TIP GAP SIZE ON THE PERFORMANCE OF AN AXIAL COMPRESSOR STAGE WITH AND WITHOUT ACTIVE FLOW CONTROL

C. Rannou - J. Marty - G. Tanguy - A. Dazin

DAAA, ONERA, Université Paris Saclay F-92190 Meudon - France
clemence.rannou@onera.fr, julien.marty@onera.fr
Univ. Lille, CNRS, ONERA, Arts et Metiers Institute of Technology,
Centrale Lille Institut, UMR 9014-LMFL,
Laboratoire de Mécanique des Fluides de Lille - Kampé de Fériet, F59000, Lille, France
antoine.dazin@ensam.eu, geoffrey.tanguy@onera.fr

ABSTRACT

The tip gap region of an axial compressor rotor is the source of complex flows inducing losses and stability issues. Recent works have proven the ability of blowing high-speed jets in the tip region to improve the surge margin of an axial compressor stage with a narrow tip gap configuration. Nevertheless, the tip gap size can evolve during the compressor lifetime, possibly affecting its performance and operability. The objective is to evaluate the performance of an active flow control system on a compressor with different tip gap sizes. The present work is based on the single stage compressor CME2 located at the Laboratory of Fluid Mechanics of Lille and equipped with actuators blowing at the rotor tip leading edge. Configurations with two different values of the tip gap to chord ratio (0.6% and 2.4%) have been experimentally tested. RANS simulations have also been performed. The effect of tip gap sizes and of the tip-blowing is evaluated on the flow topology and compressor performance.

KEYWORDS

AXIAL COMPRESSOR, ACTIVE FLOW CONTROL, SURGE MARGIN

NOMENCLATURE

A	Annulus area at the rotor inlet ($A = 0.1029\ m^2$)	α_{inj}	Injection angle (°)
ρ	Density ($\rho = 1.225\ kg/m^3$)	ΔP_s	Static pressure variation (Pa)
ϕ	Flow coefficient: $\frac{\dot{m}/\rho A}{U}$ (-)	Ψ	Pressure coefficient: $\frac{\Delta Ps}{\rho U^2}$ (-)
PB	Power Balance (%)	SBC	Single Blade Channel
RANS	Reynolds-Averaged Navier-Stokes	*SMI*	Stall Margin Improvement
β	Relative blowing angle (°)	SM	Stall Margin
P	Nominal compressor power (W)	V^*_{jet}	Jet velocity scaled (-)
Q_{inj}	Global injected mass flow rate (kg/s)	$P_{s,t}$	Static, Total Pressure (Pa)
R	Ratio (tip gap size over the axial chord)	$\dot{m}$	Mass Flow rate (kg/s)
T_t	Total Temperature (K)	U	Rotor tip velocity (m/s)

INTRODUCTION

Flow control is a key technology to improve aerodynamic performance and should be used to achieve the constraints which are imposed to aeronautical engine manufacturers in terms of

CO_2 and pollutant emissions. According to Air Transport Action Group [2021], a net-zero carbon emission is the main goal to achieve pledged by 2050. Increasing the efficiency of axial compressors is undoubtedly always a considerable challenge due to performance limitations related to instabilities such as rotating stall and surge. Rotating stall is usually developing at the clearance region between the blades and the casing and arises from the interaction of the tip leakage flow with the main flow. Therefore, control systems acting on the flow near the casing offer an efficient solution to increase the stall safety margin and thus the compressor operating range by means of passive devices (modification of the geometry without energy inputs) or active devices (need of an external energy source). Recent studies have shown that active control by injection of air upstream of the leading edge of the rotor tip, makes it possible to delay the onset of stall. Indeed, active control offers a more flexible solution unlike passive control, as it can be adapted to the machine operating point and can accommodate engine cycling and wear issues. Previous works have investigated experimentally the influence of the the main geometric and fluidic parameters having an influence on the injection performance (Suder et al. [2001], Li et al. [2020]). CFD calculations have also been used to evaluate the ability of such system to reduce losses and increase the compressor surge margin. One can cite, Marty et al. [2013] who analyzed the effect of blade tip suction and blowing or Neuhaus and Neise [2005] who focused on continuous air injection for different configurations. Nevertheless, all the above cited works focused on a fixed compressor geometry, whereas the tip clearance of a compressor evolves with the machine age, depends on the rotor location and the speed variations and whereas it is well established that a modification of the tip gap size has a strong impact on the compressor performance.

As an example, the isentropic efficiency is significantly reduced as the ratio $R\,(=\frac{\tau}{c})$, defined by the tip gap size τ over the axial chord c, is increased from 0.9% to 3.4% (Cumpsty [1989]). The operating zone is also minimized due to a reduction of almost 10% of the stall safety margin (Cumpsty [1989]). According to the work of Smith [1958], the tip gap size is inversely proportional to the peak pressure rise of a blade: for every percent of increase in the tip gap size, 4% additional pressure losses are observed.

The main goal of the present paper is to evaluate the performance of an active flow control system on a compressor with different tip gap sizes and investigate the fluid physics parameters with continuous blowing case (no forcing frequency). The support of this study is the CME2, a single stage compressor located at the Lille Fluid Mechanics Laboratory (LMFL). Previous studies have investigated experimentally and numerically the tip gap size ratio R at R = 0.6% (Marty et al. [May 2023], Moubogha et al. [2022]). Hence, the paper is presented the effect of control on a larger tip clearance defined at R = 2.4%. The paper is organised as follows: first, the test bench and the CFD methodology are described. Then, a reference case is presented. Finally, the impact of active flow control parameters is discussed.

MATERIALS AND METHODS

CME2 Active Control System

The considered test-case is the single stage low speed axial compressor CME2 located at the Lille Fluid Mechanics Laboratory. All the tests presented were performed at Ω = 3200 rpm. The numbers of blades of the rotor and the stator are respectively 30 and 40 giving a periodicity of $2\pi/10$. Stagnation pressure ratio is 1.03 at Ω, and the nominal massflow rate is equal to 5.3 kg/s. The rotor tip speed is 94 m/s. The design axial velocity at leading edge is 43 m/s.

More details about the geometrical configuration are given in Veglio [2016]. The air injection system of the CME2 consists of 40 actuators grouped in pairs on 20 blocks, evenly

distributed around the circumference of the compressor (Figure 1). The blow-off is designed to be as close as possible to the rotor blade tips and thus the injection channel is curved at the outlet. This particular shape generates an air outlet tangential to the wall: the jet remains therefore stucked to the casing wall thanks to the Coandă effect. The center of the actuators is located 10 mm from the leading edge of the rotor. Figure 1 presents the general characteristics of the active control system. The injectors are fed with an external compression system which allows to adjust the mass flow injected by the control system. The absolute injection angle is also adjustable and is defined as follow: the angle is positive (negative) when the jet tangential velocity component is in the same direction (opposite direction) as the speed of rotation (Figure 2).

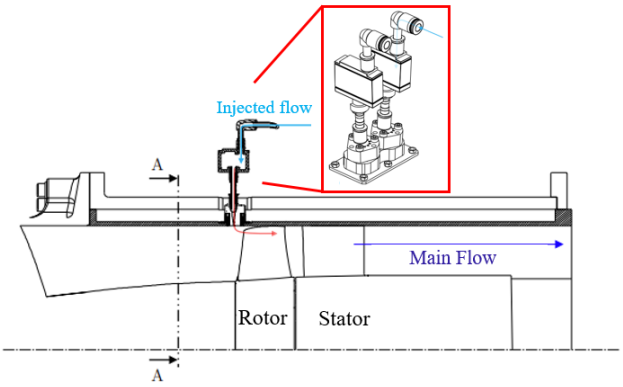

CME2 Injection System

Number of injectors	40
Axial position	-10 mm
Injection angle (pitch)	0°
Outlet section	5 mm²

Figure 1: CME2 active control system: longitudinal view (left) and setup characteristics (right)

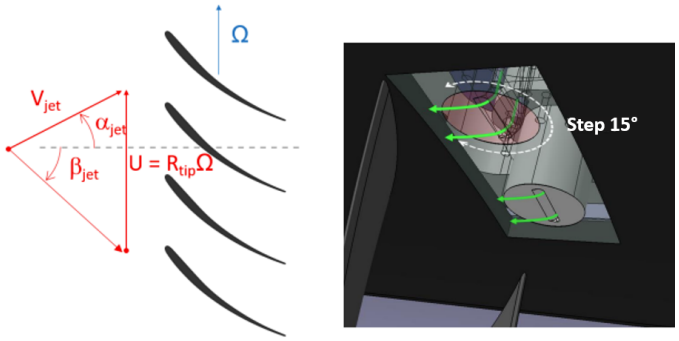

Figure 2: Definition of the absolute angle of injection and CAD view of adjustable yaw blowing angle of the injectors

Numerical Set-up

Presentation of the 2π/10 configurations

A preliminary computational domain has been designed to obtain a $2\pi/10$ configuration using the natural periodicity of the machine. It consists of a single-blade channel composed of one rotor blade and one stator blade with one pair of fluidic actuators. The mesh is composed of 3.1 10^6 nodes. The y^+ values at the blade wall are lower than 1 in the entire domain. When the tip gap size is changed, the number of points has been adjusted to maintain the cells aspect ratio. It has been presented in Rannou et al. [2022] that for the smaller tip gap (R = 0.6%), the

Single Blade Channel and $2\pi/10$ configurations are giving very similar results from nominal to stall conditions which are very close to experimental data. Nevertheless, for the larger tip gap (R = 2.4%), the SBC simulations fail to predict the critical mass flow rate at stall conditions. Hence, in the present paper the results from the RANS $2\pi/10$ configuration are presented.

Concerning the injectors, the mesh is composed of prisms / pyramids / tetrahedra at the interface between the injector and the channel (upstream, rotor and stator parts). The channel is meshed with structured blocks using a 'O-nH' topology. All the injector is meshed with hexahedra and as been processed in unstructured blocks by the software Pointwise.

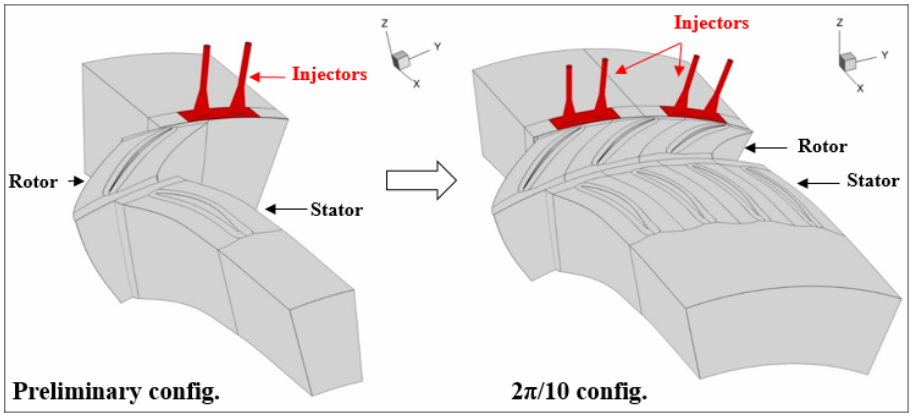

Figure 3: Preliminary and $2\pi/10$ configurations

General parameters

RANS $2\pi/10$ calculations are performed with the elsA solver, developed at ONERA and co-owned by ONERA and SAFRAN (Cambier et al. [2013]). This code relies on a cell-centered finite-volume discretization on structured and unstructured multi block meshes. A convergence study has been conducted with 10^6 and 2.10^6 nodes in order to study the compromise between computational cost and reliability in previous papers as quoted in Baretter et al. [2021]. Reynolds-Averaged Navier-Stokes equations are solved for compressible flows. Ideal gas law characterizes the fluid with the Sutherland's law for the viscosity. The heat fluxes are computed with the Fourier's law and diffusive fluxes are calculated with a classical second-order-centered scheme. Turbulence is modeled with the Spalart-Allmaras model (Spalart and Allmaras [1992]). The Roe solver is used as second order centered space discretization in order to compute the transport equations of turbulence models and the Navier-Stokes equations. Time integration is solved by a backward Euler scheme. Local time stepping is also applied to enhance the convergence rate in steady flow conditions.

The boundary conditions that have been used are summarized in Table 1. A mixing plane is used in order to resolve the rotor-stator interface and connect the rows in RANS calculations. Additionally, a subsonic outlet condition is used downstream of the domain: a static pressure is imposed with a radial equilibrium law defined by a valve law ($P_s = P_{ref} + \alpha_{relax}(\dot{m}/\dot{m}_{ref})^2$) based on a valve coefficient α_{relax} allowing to set new operating conditions with a specific massflow rate (P_{ref} = 101325 Pa, $\dot{m}_{ref}$ = 10.0 kg/s).

Different meshes have been undertaken in order to evaluate the influence of the absolute injection angle of the jets [0°; -30°] on performance at the rotation speed defined at 3200 rpm.

The considered hybrid meshes are characterized in Figure 4 illustrating the injector mesh for each injection angle α_{inj}: 0°, -30°.

Table 1: Boundary Conditions

Upstream	- Subsonic inlet condition with prescribed total pressure
	- Axial flow direction, P_t = 101325 Pa, T_t = 288.15 K
Blades, casing, hub	- Adiabatic wall condition
	- Fixed wall condition for casing and a part of the hub
	- Mobile wall condition for hub and blades
Downstream	- Subsonic outlet condition with radial equilibrium using a valve law on static pressure
Inlet of the injector	- Subsonic inlet condition with prescribed mass flow rate, Q_{inj}
	- Flow direction normal to boundary, T_t = 288 K
Injectors walls	- Adiabatic wall conditions

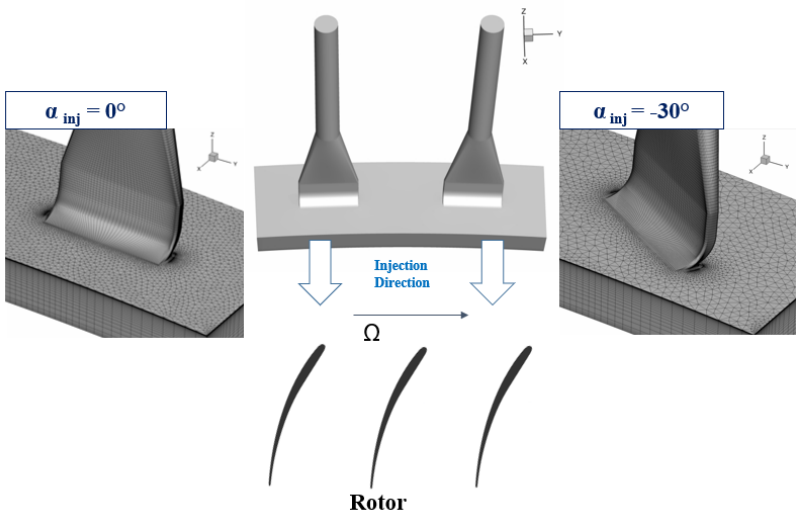

Figure 4: Different mesh configurations at α_{inj} = 0°, -30°

RESULTS AND DISCUSSION

Reference without control: baseline performance assessment

First to assess agreement between experimental data and numerical results, simulations have been performed without control with $2\pi/10$ configurations for a narrow tip gap size at R = 0.6% and a larger one at R = 2.4%. Experimentally, tests have been conducted on the CME2, on both tip gap sizes without control and by throttling progressively a valve from nominal to stall conditions. For R = 0.6%, the experimental data are issued from Moubogha et al. [2022]. As a

reference case, simulations have been compared at the same configuration of the baseline of the experimental data with injectors oriented at α_{inj} = 0° without blowing (Figure 5).

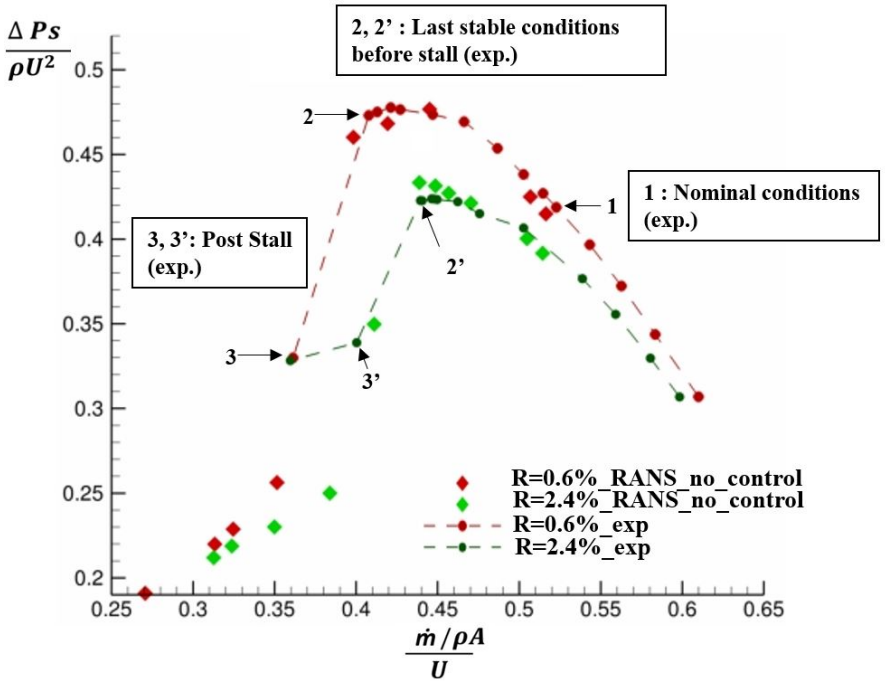

Figure 5: CME2 performance map at two tip gap sizes (R = 2.4% and R = 0.6%) for configuration with injectors at α_{inj} = 0° without blowing for experimental tests and numerical results

Specific operating conditions for ratio R = 0.6% and R = 2.4%

The design compressor flow coefficient is 0.53. The critical flow rate for which the compressor encounters stall is 0.41 and 0.44 at respectively R = 0.6% and R = 2.4%. The simulations investigate a range of mass flow rates from 0.25 to 0.53. Among the conditions considered, several operating points are identified as follow: i) Nominal conditions ($\phi_1 = 0.53$), ii) Last stable conditions before stall: the last experimental point (S) before a clear break in the slope of the performance curve (at ϕ_{S2} and $\phi_{S2'}$), iii) Post-stall conditions at lower massflow rate than ϕ_S.

Results from nominal to the last stable conditions at ratio R = 0.6% and R = 2.4%

The performance chart is provided with the RANS numerical results for the two tip gap sizes (R = 0.6% and R = 2.4%) and with experimental data. The $2\pi/10$ simulations provide excellent results when it is compared with the experimental data at R = 0.6%. Especially, it gives discrepancies less than 1% to the last stable conditions for R = 0.6%, even if the numerical results slightly underestimate $\Psi = \frac{\Delta Ps}{\rho U^2}$ from ϕ = 0.53 to ϕ = 0.45. Similarly, for R = 2.4% the numerical results give acceptable performance data at this larger tip clearance. Indeed, from ϕ = 0.53 to ϕ = 0.45, RANS $2\pi/10$ simulations produce discrepancies less than 1%. The largest deviation from experimental data is related to the conditions close to stall. For R = 0.6%, the experimental critical mass flow rate is ϕ_{S2}= 0.41 whereas the numerical simulation are predicting the slope discontinuity characteristics at ϕ_S= 0.39. Moreover, the numerical results slightly underestimate Ψ compared to experimental data at the top of the curve, but it captures

well the same trend of performance just before stall. In the same way, for R = 2.4%, RANS results seem to define a last stable point at lower massflow rate but close to $\phi_{S2'} = 0.44$. The compressor pressure rise just before stall is slightly over-evaluated.

Performance of flow control at different tip gap sizes

The impact of the active flow control is investigated in continuous blowing at 3200 RPM with 40 injectors activated at R = 0.6% and 2.4%, with an injection angle set to α_{inj} = -30°. This absolute injection angle was chosen as a reference for R = 0.6% as it corresponds to the optimal performance of the compressor in terms of stall margin improvement according to Moubogha et al. [2022].

The experimental and numerical compressor performance maps are presented in Figure 6. The blowing flow rate is set in the simulation to Q_{inj} = 2.0% to correspond to the experimental results. The injected massflow rate Q_{inj} is defined as a percentage of the compressor massflow rate at the last operating point without control for the nominal geometry R = 0.6%. If the last operating point without control for R = 2.4% is chosen, a slight discrepancy of 0.025% is observed, that is why to compare each case, R = 0.6% is taken as a reference. Moreover, according to Margalida et al. [2021], the injected mass flow rate in each pair of injector valve was observed constant with a slight variation of 1%, regardless of the pair considered.

As already observed experimentally in Moubogha et al. [2022] and Margalida et al. [2021], for R = 0.6% the control system proves its capacity to push the stability limit to lower flow rates (ϕ_S is decreased from 0.41 to 0.32) and improves the static pressure rise of the compressor. At the largest gap size R = 2.4%, the effect of blowing is even more efficient as the stall limit with control is $\phi_S = 0.335$, very close to the one observed for the narrow gap size. Moreover, compared to the baseline characteristic curves, the controlled curves present an increase of the static pressure ratio with a slope of the curves becoming positive especially for R = 2.4%.

Concerning CFD predictions, the static pressure drop is also delayed to lower massflow rates compared to the cases with no control for both tip clearances. The $2\pi/10$ simulations permit to give a similar controlled performance trend but it underestimates Ψ when the experimental data curves flattens to the top from $\phi = 0.4$ to $\phi_S = 0.335$ for R = 2.4% and from $\phi = 0.41$ to $\phi_S = 0.32$ for R = 0.6%. This means that the $2\pi/10$ simulations are sufficient to predict the change of slope when stall occurs with blowing control but with a lack of accuracy for the sudden static pressure drop captured with the experiments. Unsteady simulations of the compressor with 360° configuration should capture the effect of blowing with further accuracy when the massflow rate is getting close to stall.

To illustrate the effect of blowing on the flow near casing, the slices of static pressure at 96% of rotor blade height for specific operating conditions are plotted (Figure 7). It can be noticed some variation in the intensity between the two configurations with and without control. For the configuration without control, a characteristic low relative pressure region at the leading edge is observed. This specific static pressure drop region is associated to the tip leakage vortical flow. At the last stable point without control, the picture highlights the modification of incidence of the tip leakage vortex with the nominal case, as it moves toward the leading edge. At stall conditions, there is a drop in static pressure variation shown in the performance map and the tip leakage vortex is no longer visible longer, as the flow is detached. When the blowing is activated, at each operating condition, this lower static pressure region seems to be confined along the suction side of the rotor, avoiding the compressor to stall at ϕ = 0.44. This suggests that the CFD is able to capture the main effect of blowing on the leakage flow and its effect to delay stall.

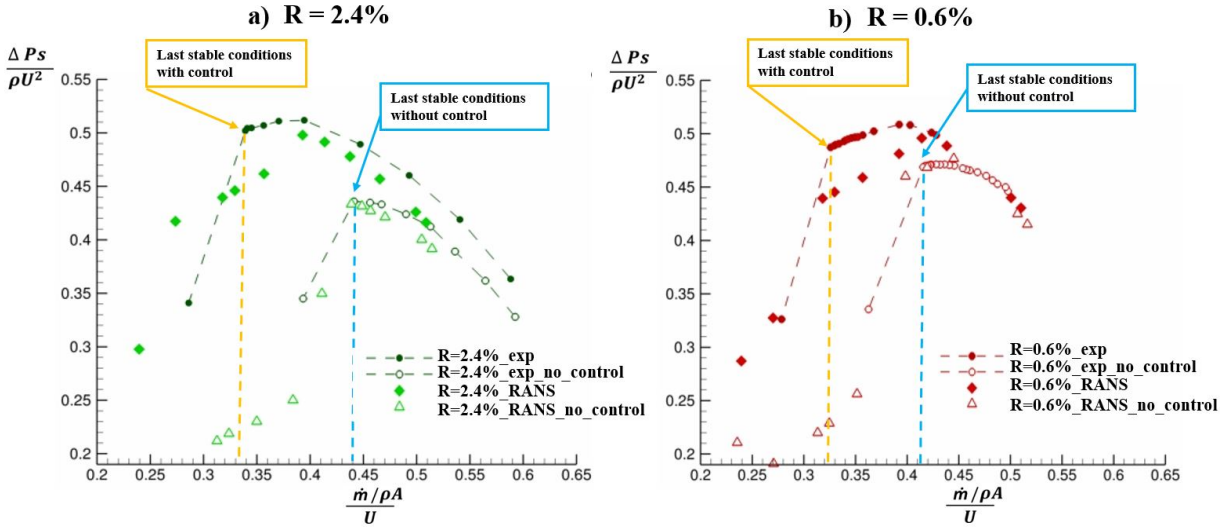

Figure 6: CME2 performance map at R = 2.4% and at R = 0.6% with α_{inj} = -30° ($Q_{inj} = 2.0\%$)

To characterize the effect of the control system on the compressor performance, two parameters are introduced: the power balance (Moubogha et al. [2022]) and the *SMI* presented by Weigl and al [1997]. The mass averaged power balance is defined as the additional total power provided to the flow by the compressor due to the control. The total pressure at inlet includes the jets dynamic pressure. It can be simply defined by the net benefit (energy gain in terms of pressure rise of the compressor stage - energy cost due to the blowing system) of the control system.

$$\overline{PB} = \frac{\left((Q_{\mathrm{S,B}} + Q_{\mathrm{inj}})\frac{\Delta p_{\mathrm{tt,C,int}}}{\rho_{\mathrm{C}}}\right) - \left((Q_{\mathrm{S,B}})\frac{\Delta p_{\mathrm{tt,B}}}{\rho_{\mathrm{B}}}\right)}{P} \times 100 \tag{1}$$

with P, Q, Δp_{tt}, the compressor nominal power (P = 23,000 W), the mass flow rate and the total-to-total pressure rise. The subscripts B, C, S, inj, int refer to: the baseline case without control, the controlled case, the last stable operating point with the lowest flow rate before stall, injected for the global injected mass flow rate, and interpolated for the controlled total-to-total pressure.

With the similar nomenclature, the *SMI* is determined by the ratio of the surge margin with control, SM_{C}, and without control, SM_{B} (Figure 8 a)):

$$SM_{\mathrm{B}} = ((\frac{\Delta p_{\mathrm{tt,B}}}{Q_{\mathrm{S,B}}})(\frac{Q_{\mathrm{nom}}}{p_{\mathrm{nom}}}) - 1) \times 100 \tag{2}$$

$$SM_{\mathrm{C}} = ((\frac{\Delta p_{\mathrm{tt,C}}}{Q_{\mathrm{S,C}}})(\frac{Q_{\mathrm{nom}}}{p_{\mathrm{nom}}}) - 1) \times 100 \tag{3}$$

$$SMI = \frac{SM_{\mathrm{C}} - SM_{\mathrm{B}}}{SM_{\mathrm{B}}} \times 100 \tag{4}$$

It has to be noted that, on the contrary to Moubogha et al. [2022], the total pressure at inlet, in the controlled case, is including the energy added by the jets. Figure 8 b) offers a *SMI* vs power balance comparison between the two tip clearances at α_{inj} = -30° with configurations with control at 20 injectors and at 40 injectors. Different Q_{inj} have been tested with a range from

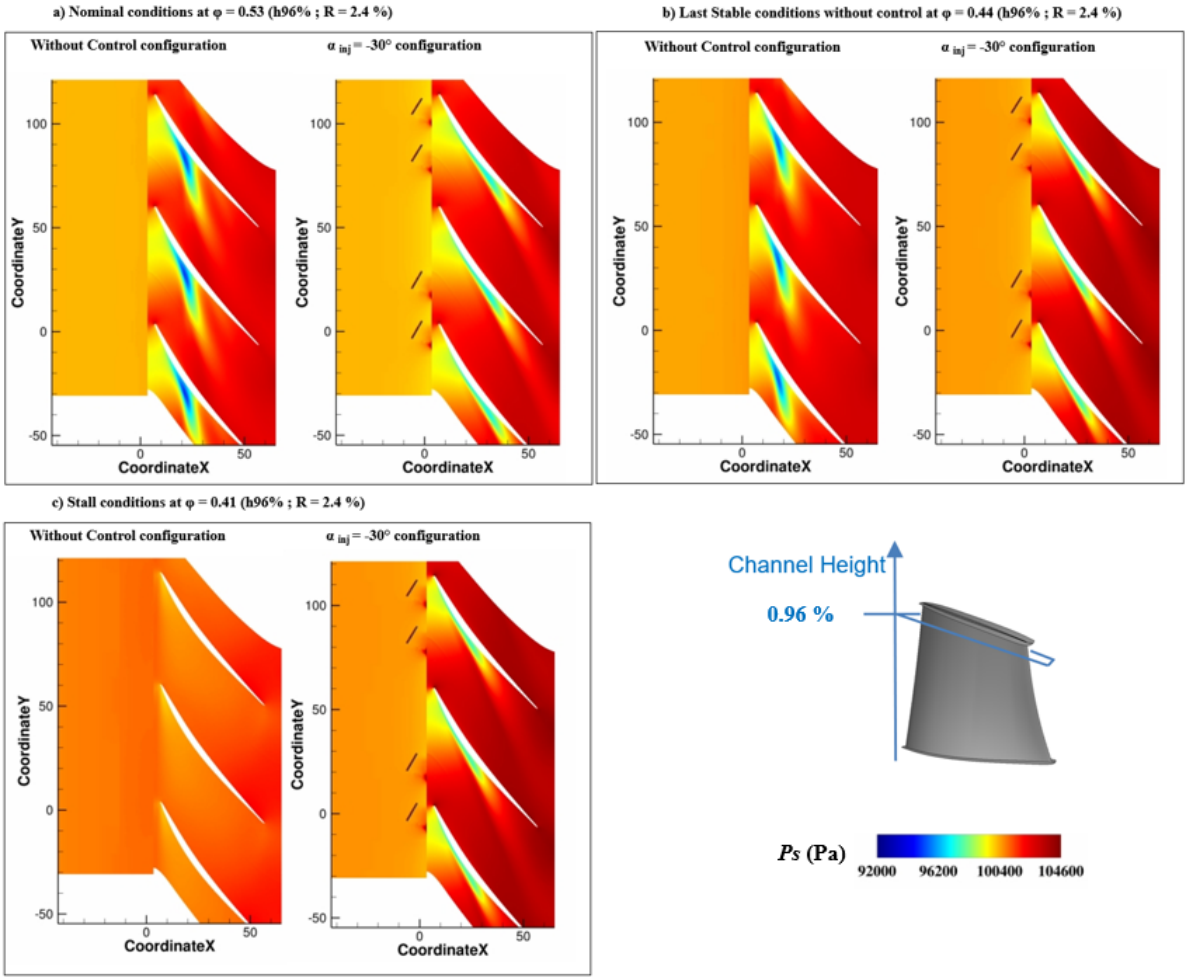

Figure 7: Static pressure field for R = 2.4% at nominal, last stable and stall conditions with configurations: without control and with control (α_{inj} = -30° and $Q_{inj} = 2.0\%$)

Q_{inj} = 0.5% to Q_{inj} = 2.5%. The interesting configurations are the ones achieving significant *SMI* and positive power balance. That means that the control parameters allowing this results target points on the top and/or the right of the map. According to this, it appears that the configurations with 40 injectors offer the best results for each tip clearance size compared to 20 injectors. Consequently, it allows an acceptable angular coverage around the circumference of the compressor. The cases at Q_{inj} = 1 and 1.5% offers interesting applicative configurations as it permits to obtain a satisfied *SMI* and a positive power balance reaching 5.8 % of the compressor nominal power. The cases at Q_{inj} = 2.5% correspond to the maximum energetic cost as it represents the maximum number of injectors with the maximum flow rate per injector. Additionally, at R = 2.4%, the *SMI* is provided excellent results compared to R = 0.6% allowing *SMI* and power balance up to nearly 200% and 6% respectively. Nevertheless, it has to be kept in mind that the *SMI* is calculated by taking the last stable point from the baseline case without control as shown on Figure 6: the baseline at R = 2.4% is lower than the one at R = 0.6%, due to the higher losses that happen between the carter and the rotor blade with a lower height.

Finally, it has been shown that the active control with α_{inj}= -30° seems to be efficient as it postpones stall limit with a stall massflow rate decrease and a pressure ratio increase. It improves the *SMI* offering a possible strategy stabilizing the tip gap region.

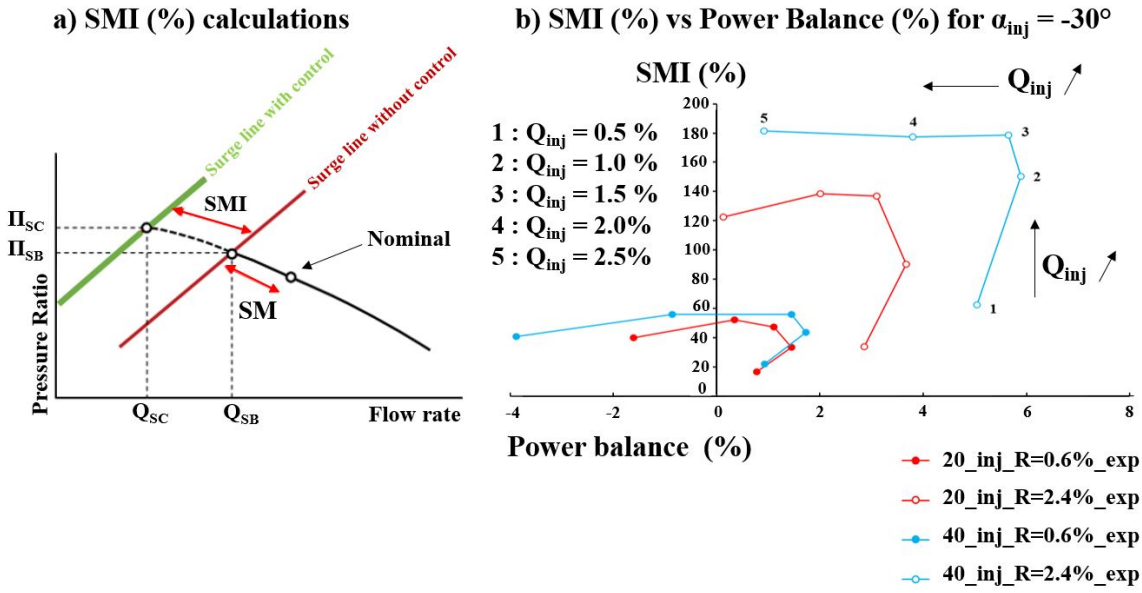

Figure 8: a) *SMI* calculations and b) *SMI* (%) and power balance (%) of the control system with experimental data at R = 0.6% and 2.4% for α_{inj} = -30° with 20 and 40 injectors

Impact of the injection control parameters

Further configurations have been explored experimentally with different control parameters. In this section, the active flow control in continuous blowing at 3200 RPM have been tested with 40 and 20 injectors activated and various absolute flow angles: the performance curves are presented with α_{inj} = 0°, -30°, -45°, -60° at $Q_{inj} = 1.5\%$ (Figure 9). For configurations with 40 injectors, the best results are obtained for α_{inj} = -45°, and with 20 injectors, for α_{inj} = -30°. Indeed, the effect of blowing control generates higher static pressure prise at these angles. In addition, the stall onset is delayed, especially for a 40 injectors configuration.

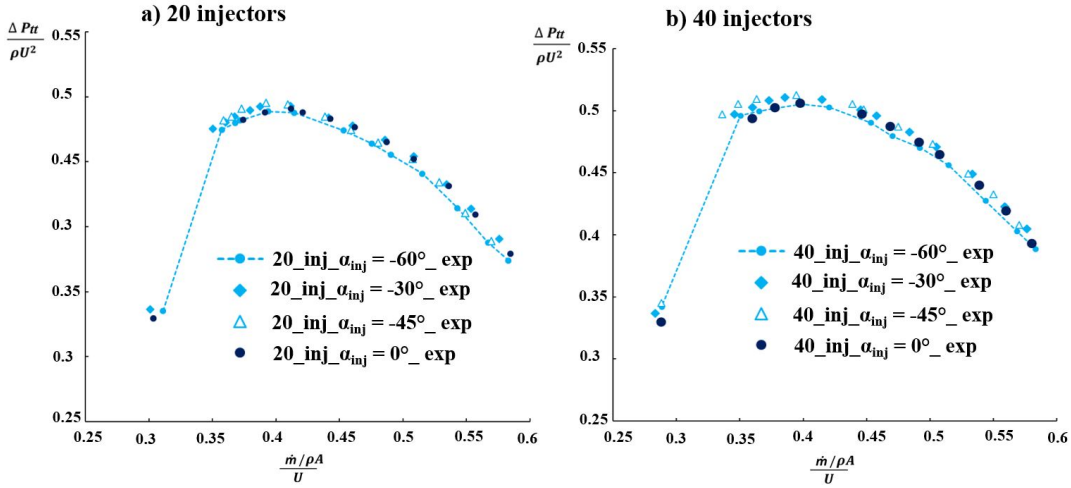

Figure 9: CME2 performance map at R = 2.4% at 0°, -30°, -45°, -60°: with a) 20 injectors and b) 40 injectors

The global performance of the other fluidic parameters is then analyzed focusing on the

configurations with 40 injectors as this configuration produces the best results in terms of performance. In Figure 10 a), the power balance vs *SMI* is investigated for the continuous blowing at specific angles of injection. As expected, blowing control configurations allow to provide the best *SMI* with a high positive power balance with α_{inj} = -45°, especially for the injected massflow rates at Q_{inj} = 1 and 1.5%. Consequently, it seems that for a larger tip gap size, the best configuration for active control is obtained with 40 injectors at α_{inj} = -45°. In Figure 10 b), the *SMI* is reported as a function of the relative blowing angle β. The results are extracted for different values of V^*_{jet} defined by the jet velocity scaled by the rotor tip blade velocity (U). The *SMI* clearly presents maxima for a relative blowing angle around 60°. In a previous study (Moubogha et al. [2022]), it was already mentioned that, for R = 0.6%, this value of the relative blowing angle which corresponds approximately to the inlet blade angle at tip for the CME2 compressor allows to obtain the best *SMI*.

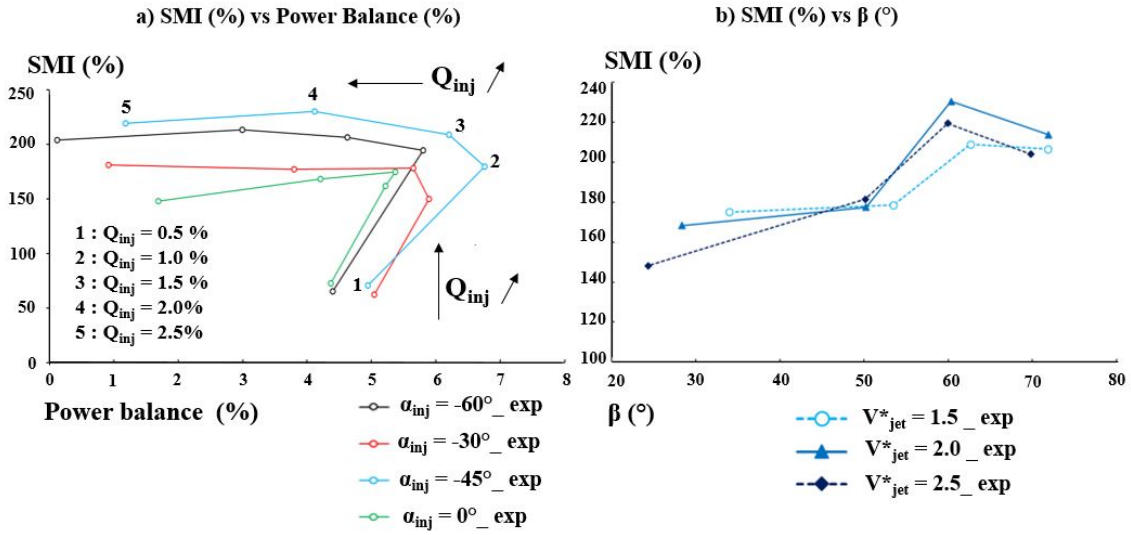

Figure 10: a) *SMI* and power balance b) *SMI* (%) and β (°) at R = 2.4% for α_{inj} = 0°, -30°, -45°, -60° with 40 injectors

CONCLUSIONS

The present study reports the effect of active flow control on a narrow and a large tip gap sizes. The experimental campaign has been conducted on a single stage axial compressor test-bench, equipped with fluidic actuators around the circumference. Measurements were performed from design conditions to operating points close to stall for configurations with and without control.

Compared with previous studies carried out for a narrow tip gap size on CME2 test bench, the present work highlights the benefit of active flow control on a large tip gap size: for this configuration, the impact of blowing allows a great delay of stall onset (*SMI* of the order of 200%), and a pressure rise increase allowing a net positive power balance of the system. The study has evidenced the optimal configurations for blowing, implying a specific injection angle and full injectors activated around the compressor circumference. For larger tip gap size, it seems that the air injection limits better the losses induced by the tip gap flow, generating a higher *SMI* than for narrow tip clearance. Further experimental tests should enhance the analysis of the development of stall with active control thanks to unsteady measurements and

attest the efficiency of tip blowing leading to the stabilization of the tip gap flow.

In parallel, RANS $2\pi/10$ simulations were achieved for the same configurations. The RANS $2\pi/10$ simulations are predicting rather accurately the performance map without control and are able to catch qualitatively the performance improvement induced by the control system. The analysis of the static pressure maps close to the casing have shown that the blowing is confining the tip leakage flow near to the blade wall. Hence, this contributes to delay stall. Full annulus calculations using URANS should provide further performance comparisons and flow topology assessments.

ACKNOWLEDGEMENTS

The authors wish to thank the Consortium Research-Industry in Turbomachinery (CIRT) grant supporting the study and also the members of ACONIT project for providing numerical database. The authors would like to thanks the french Defence Innovation Agency (AID) for co-funding this PhD. All simulations have been performed in the framework of the elsA agreement between SAFRAN and ONERA, which are co-owners of this software.

REFERENCES

K. L. Suder, M. D. Hathaway, S. A. Thorp, A. J. Strazisar, and M. B. Bright. Compressor stability enhancement using discrete tip injection. *J. Turbomach*, 123:14, 2001.

J. Li, J. Du, S. Geng, F. Li, and H. Zhang. Tip air injection to extend stall margin of multi-stage axial flow compressor with inlet radial distortion. *Aerospace Science and Technology, Elsevier Masson SAS*, 96:105554, 2020. doi: doi: 10.1016/j.ast.2019.105554.

J. Marty, L. Castillon, J-C. Boniface, S. Burguburu, and A. Godard. Numerical and experimental investigations of flow control in axial compressors. *AerospaceLab Journal*, 6:1-13, 2013. doi: 10.12762/2013.AL06-09.

L. Neuhaus and W. Neise. Active control to improve the aerodynamic performance and reduce the tip clearance noise of axial turbomachines. *In AIAA Aeroacoustics Conference*, 2005.

N. A. Cumpsty. Compressor aerodynamics. *Longman Scientific & Technical*, 1989.

H.Jr Smith. The effect of tip clearance on the peak pressure rise of axial flow fans and compressors. *In ASME symposium on stall, American Society of Mechanical Engineers*, pages 149–152, 1958.

J. Marty, L. Castillon, and P. Joseph. Numerical investigations on the rotating stall in an axial compressor and its control by flow injection at casing. *ASME. J. Turbomach.; 145(5): 051009*, May 2023. https://doi.org/10.1115/1.4056090.

J. Moubogha, G. Margalida, P. Joseph, O; Roussette, and A. Dazin. Surge margin improvement by continuous and pulsed tip injection. *Int. J. Turbomach. Propuls. Power*, 7, 10, 2022. https://doi.org/10.3390/ijtpp7010010.

M. Veglio. *Etude expérimentale et numérique des écoulements dans un étage de compresseur axial à basse vitesse en régime de fonctionnement instable.* PhD Thesis, ENSAM, HAL Id: fftel-01345795, 2016.

C. Rannou, A. Dazin, J. Marty, G. Tanguy, L. Castillon, and J. Moughoba. Effect of the axial compressor tip clearance size: Performance and transition to rotating stall. *Proceedings of ASME Turbo Expo 2022, Turbomachinery Technical Conference and Exposition (GT2022-80914)*, 2022.

L. Cambier, S. Heib, and S. Plot. The Onera *elsA* CFD software: input from research and feedback from industry. *Mechanics & Industry*, 14:159–174, 1 2013. ISSN 2257-7750. doi: 10.1051/meca/2013056.

A. Baretter, B. Godard, P. Joseph, O. Roussette, F. Romano, R. Barrier, and A. Dazin. Experimental and numerical analysis of a compressor stage under flow distortion. *Int. J. Turbomach. Propuls. Power*, 6(43):621–656, 2021. doi: 10.3390/ijtpp6040043.

P.R. Spalart and S.R. Allmaras. A one-equation turbulence model for aerodynamic flow. *In 30th Aerospace Science Meeting & Exhibit.*, pages 92–0439, 1992. AIAA.

G. Margalida, P. Joseph, O. Roussette, et al. Active flow control in an axial compressor for stability improvement: on the effect of flow control on stall inception. *Experiments in Fluids*, 62(12), 2021. https://doi.org/10.1007/s00348-020-03104-4.

H. J. Weigl and al. Active stabilization of rotating stall and surge in a transonic single stage axial compressor. *In ASME Int. Gas Turbine Aeroengine Congr. Exhib. Proceeding, vol. 4*, 1997.

Air Transport Action Group. Waypoint 2050. *https://www.atag.org/*, 2021.